Tenascin-C preserves microglia surveillance and restricts leukocyte and, more specifically, T cell infiltration of the ischemic brain

Daniel Manrique-Castano [a,1], Egor Dzyubenko [a,1], Mina Borbor [a], Paraskevi Vasileiadou [a], Christoph Kleinschnitz [a], Lars Roll [b], Andreas Faissner [b,*], Dirk M. Hermann [a,*]

[a] Department of Neurology, University Hospital Essen, Hufelandstraße 55, D-45122 Essen, Germany
[b] Department of Cell Morphology and Molecular Neurobiology, Faculty of Biology and Biotechnology, Ruhr University Bochum, Universitätsstraße 150, D-44801 Bochum, Germany

ARTICLE INFO

ABSTRACT

As an endogenous activator of toll-like receptor-4 (Tlr4), the extracellular matrix glycoprotein tenascin-C (TnC) regulates chemotaxis, phagocytosis and proinflammatory cytokine production in microglia. The role of TnC for ischemic brain injury, post-ischemic immune responses and stroke recovery has still not been evaluated. By comparing wild type and $TnC^{-/-}$ mice exposed to transient intraluminal middle cerebral artery occlusion (MCAO), we examined the effects of TnC deficiency for ischemic injury, neurological deficits, microglia/macrophage activation and brain leukocyte infiltration using behavioural tests, histochemical studies, Western blot, polymerase chain reaction and flow cytometry. Histochemical studies revealed that TnC was *de novo* expressed in the ischemic striatum, which contained the infarct core, and overlapped with the area of strongest accumulation of Iba1 + microglia/macrophages. TnC deficiency increased overall Iba1 immunoreactivity in the perilesional cortex, suggesting that TnC might restrict the distribution of microglial cells to the infarct core. By analysing microglial morphology in 3D we found that the post-ischemic loss of microglial cell territory, branching and volume at 3 and 7 days post-ischemia was amplified in the brains of TnC deficient compared with wild type mice. Microglial cell number was not different between genotypes. Hence, TnC deficiency reduced tissue surveillance by microglial cells. Concomitantly, the number of infiltrating leukocytes and, more specifically, T cells was increased in the ischemic brain parenchyma of TnC deficient compared with wild type mice. Ischemic injury and neurological deficits were not affected by TnC deficiency. We propose that the reduced microglia surveillance in TnC deficient mice might favour leukocyte accumulation in the ischemic brain.

1. Introduction

Immune responses play a central role in modulating brain injury and recovery post-stroke (Anrather and Iadecola, 2016; Jayaraj et al., 2019). Post-ischemia, complex cellular and molecular mechanisms are triggered in the brain, including the release of inflammatory cytokines and alarmins by damaged cells (Bianchi, 2007; Roth et al., 2018), neuroglia activation and the brain invasion of leukocytes belonging to the innate and adaptive immune systems (Gelderblom et al., 2009; Neumann et al., 2015). Immune cell trafficking across the blood–brain barrier is mediated by adhesion molecules including intercellular adhesion molecule-1 (ICAM1) and vascular cell adhesion molecule-1 (VCAM1) (Lopes Pinheiro et al., 2016), but their migration within brain parenchyma remains poorly understood. In ischemic stroke, both peripheral leukocytes and resident microglia have to navigate across the extracellular space along a modified extracellular matrix (ECM). Based on the available data, we previously suggested that the interactions between immune cells and the ECM could crucially influence neurological recovery post stroke (Dzyubenko et al., 2018). In this study, we addressed the role of ECM glycoprotein tenascin-C (TnC), a potent regulator of cell migration, in post-ischemic neuroinflammation.

TnC is a multifunctional glycoprotein that is highly expressed in the developing central nervous system (CNS) (Faissner et al., 2017). The multitude of binding partners and isoforms makes TnC an ubiquitous participant of cell–cell interactions. In the adult brain, TnC expression is normally restricted to the stem cell niches (Kazanis et al., 2007), but can

---

be upregulated in response to mechanical injury (Laywell et al., 1992). As an endogenous activator of toll-like receptor-4 (Tlr4), TnC controls inflammation (Midwood et al., 2009; Wiemann et al., 2019). In the brain, the activation of Tlr4 by TnC was recently shown to regulate chemotaxis, phagocytosis and proinflammatory cytokine production in microglia (Haage et al., 2019). Since Tlr4 mediated activation of microglia is an essential component of neuroinflammation (Caso et al., 2007), we hypothesized that TnC regulates secondary brain injury after stroke. Although recent studies highlighted the importance of TnC in models of retinal ischemia and subarachnoid haemorrhage (Reinhard et al., 2017; Shiba and Suzuki, 2019), its potential role in the ischemic brain was not investigated to our knowledge. In a model of transient middle cerebral artery occlusion (MCAO), we here evaluated the effects of genetic TnC deficiency on post-ischemic immune responses, infarct size, neuronal death, neurological deficits, microglia morphology and immune cell infiltration of the ischemic brain.

2. Material and methods

2.1. Legal issues and animal housing

This study was conducted with governmental approval (Bezirksregierung Düsseldorf; project G4585/16) in accordance with E.U. guidelines for the Care and Use of Laboratory Animals (Directive 2010/63/EU), and reported based on Animal Research: Reporting of *In Vivo* Experiments (ARRIVE) guidelines. The animals were housed in groups of 3–5 individuals per cage in a 12 h:12 h human light/dark cycle with water and food *ad libitum*.

2.2. Experimental design and animal groups

In 119 male wild type (WT) and 110 TnC$^{-/-}$ mice on 129/Sv background (Forsberg et al., 1996) aged 8–12 weeks (23–28 g), we induced focal cerebral ischemia by transient intraluminal MCAO. Subsequently, we evaluated the neurological deficits and sacrificed animals at 1, 3, 7 and 42 days post-ischemia (DPI). Control group included healthy (that is, surgery-naive) WT and TnC$^{-/-}$ mice, 7 animals per genotype. The genotypes of mice were determined by PCR using following primers: tnc_low (ttctgcaggttggaggcaac), tnc_up (ctgccaggcatctttctagc) and tnc_neoup (ctgctctttactgaaggctc), followed by electrophoresis in 2% agarose gel (Supplementary Fig. 1). The groups were randomly assigned and animal numbers were as follows: flow cytometry (n = 6–7 per time-point/genotype), histochemistry/ immunohistochemistry (n = 11–12 per time-point/genotype), Western blot and RT-qPCR (n = 6 per time-point/genotype).

2.3. Experimental procedures, neurological score and animal sacrifice

Left-sided MCAO was induced by occlusion of the middle cerebral artery for 35 min using an intraluminal monofilament technique, as described previously (Dzyubenko et al., 2018). In our hands, this procedure produces localized striatal infarcts in the territory of the middle cerebral artery (bregma level 1.54 mm to −0.70 mm). During the surgery, mice were anesthetized with 1.5% v/v isoflurane (30% v/v O$_2$, remainder N$_2$O) and body temperature was kept at 37 °C using a rectal probe and a feedback-controlled heating system (Homeothermic Monitoring System, Harvard Apparatus, Harvard, USA). Cerebral blood flow in the territory of the MCA was monitored with a transcranial laser Doppler flowmeter (Perimed, Jarfalla, Sweden). During the first three days post-ischemia, mice were daily weighted and injected with 4 mg/kg carprofen (Bayer Vital, Leverkusen, Germany). General and focal neurological deficits were evaluated at 1, 3 and 7 DPI using Clark's neurological score (Clark et al., 1997). Mice losing more than 20% of body weight were sacrificed according to predefined exclusion criteria in line with requirements of the Landesamt für Natur, Umwelt und Verbraucherschutz (LANUV) Recklinghausen. Mice were sacrificed

under deep isoflurane anesthesia by transcardial perfusion with 0.9% normal saline followed by 4% v/v paraformaldehyde (PFA) in 0.1 M tris buffer saline, pH 7.2 (TBS) (animals used for histochemistry) or transcardial perfusion with 0.9% normal saline (animals used for all other studies). The brains were dissected, post-fixed overnight in 4% PFA and cryoprotected by immersing in 15% w/v and 30% w/v sucrose sequentially. 30 μm thick coronal sections were obtained using a microtome cryostat (CM1800; Leica Biosystems, Nussloch, Germany) and mounted onto pre-cooled microscope slides (J1800AMNT; ThermoFisher Scientific, Waltham, USA). Brain sections were stored at −80 °C until use.

2.4. Infarct volumetry

For infarct volumetry, brain sections taken at 500 μm intervals across the brain were stained with cresyl violet as described previously (Paul et al., 2008) and documented with a digital scanner (CanoScan LIDE 220, Canon, Uxbridge, UK). In animals sacrificed at 1, 3 or 7 DPI, infarct areas were determined by subtracting areas of healthy brain tissue of the ischemic hemisphere from those of the contralateral hemisphere as described previously (Wang et al., 2020). The infarct volume (IV) was estimated as IV = Σ(IA*Δ), where IA is the infarcted area on a section and Δ is the interval between sections. In animals sacrificed at 42 DPI, atrophy areas were determined by subtracting areas of surviving tissue in both hemispheres across the brain, of which atrophy volume (AV) was calculated as AV = Σ(AA*Δ), where AA is the atrophy area on a section and Δ is the interval between sections. At the latter time-point, the infarct is completely resolved (Wang et al., 2018). Injury analysis therefore requires volume measurements of surviving brain tissue.

2.5. Immunohistochemical procedures

Neurons, microglia, leukocytes, blood vessels and adhesion molecules were immunohistochemically detected using antibodies against NeuN (ABN91; Millipore), Iba1 (019–19741; Wako and ab5076; Abcam), CD45 (550539; BD Pharmingen), CD31 (ab28364; Abcam), ICAM1 (AF796; R&D Systems), Ki67 (ab15580; Abcam) and TnC (Kaf14; self-made, (Faissner and Kruse, 1990)). Details of the primary and secondary antibodies are provided in Supplementary Table 1. In brief, sections collected in the core of the middle cerebral artery territory (bregma level 1 to 0 mm) were permeabilized and blocked in a 0.1 M TBS buffer containing 0.1% Triton X-100, 10% donkey serum and 1% bovine serum albumin (BSA). Sections were incubated overnight at 4 °C in primary antibodies diluted in 0.1 M TBS containing 0.1% Tween-20 and 5% donkey serum, followed by immersion in secondary antibodies diluted in the same buffer for 1 h at room temperature. Brain sections were embedded in fluorescence-preserving mounting medium (FluoromountG, SouthernBiotech, Birmingham, USA).

2.6. Wide field microscopy and cell marker quantification

For the analysis of Iba1 and CD45 markers, we performed widefield microscopy using the AxioObserver.Z1 epifluorescence microscope (objective Plan-Apochromat 10×/0.45 M25; Zeiss, Jena, Germany) using the same settings for all samples. The tiling mode was applied to cover the complete striatum and perilesional cortex. The images were processed using standard ImageJ (NIH, USA) tools to obtain binary masks representing Iba1 and CD45 immunoreactivity areas (referred to as Iba1 and CD45 masks, respectively). The percentage of Iba1 labelled area was quantified in 416.7 × 416.7 μm regions of interest (ROIs) as area (Iba1 mask)/ area (total) ratio and represented the abundance of microglia/macrophages. The percentage of CD45 labelled area was quantified in the same ROIs as area (CD45 mask – Iba1 mask)/ area (total) ratio and represented the abundance of CD45^{high}/Iba1^{low} leukocytes. For each animal, we measured the average of three ROIs in striatum (dorso-lateral, dorso-medial and ventro-lateral) and cortex

(layers 3–6 of primary motor area, primary and supplementary somatosensory areas). Neuronal cell death was analysed in corresponding ROIs using terminal deoxynucleotidyl transferase dUTP nick end labelling (TUNEL) (In Situ Cell Death Detection Kit, 11684795910; Roche, Basel, Switzerland) in combination with anti-NeuN immunohistochemistry. The density of TUNEL$^+$ and TUNEL$^+$/NeuN$^+$ cells was quantified in three ROIs per animal.

2.7. Confocal microscopy and microglia morphology analysis

In representative ROIs in the ischemic striatum, confocal microscopy was performed using the Leica SP8 confocal microscope (objective HC PL APO CS2 63×/1.30, Leica Microsystems, Wetzlar, Germany) to evaluate the three-dimensional morphological features of Iba1$^+$ microglia/macrophages. Z-stacks measuring $184.52 \times 184.52 \times 15$ μm were obtained at 0.5 μm interslice distance. To analyze the 3D morphology of Iba1$^+$ cells, background and artefacts were supressed with standard ImageJ tools using fully automated scripts to avoid experimenter's bias. The analysis of 3D cell morphology was conducted using the 3DMorph software (York et al., 2018). In brief, the cell objects were detected by automated threshold setting and segmentation. After skeletonization, morphological metrics defining cell territory, cell volume, ramification index and number of branching points were derived. To our knowledge, this is the first workflow that provides the opportunity to discriminate single microglia cells in densely packed brain lesions, allowing for the precise quantification of cell morphology.

2.8. Colocalization analysis

To analyse the colocalization of adhesion molecule ICAM1 with microglia/macrophages (expressing Iba1) and blood vessels (expressing CD31), maximum intensity projections of z-stacks $184.52 \times 184.52 \times 15$ μm were obtained with the Leica SP8 confocal microscope. Using the EzColocalization plugin for ImageJ (Stauffer et al., 2018), the Manders Colocalization Coefficient (MCC) for the marker pairs ICAM1/Iba1 and CD31/ICAM1 was computed. For threshold determination, the Costes method was applied.

2.9. Western blot

Ischemic hemispheres containing the infarct were carefully separated, manually homogenized using a surgical forceps and quickly frozen at −80 °C. For RNA extraction, the samples were immersed in Trizol (15596018; Thermo Fisher Scientific) and vigorously triturated using a syringe. After homogenization, 1:5 v/v chloroform was added, followed by vortexing and incubation at room temperature for 3 min. Thereafter, samples were centrifuged at $12,000g$ for 20 min at 4 °C. The transparent aqueous fraction was collected for mRNA isolation, and the remaining pellet was used for protein extraction. Sections were incubated in 750 μl of 100% ethanol complemented with 200 μl of bromochloropropane and 600 μl of Milli-Q water. Subsequently, the samples were gently mixed and centrifuged at 13,400 rpm for 5 min at 4 °C. The upper layer was discarded, 1000 μl of 100% ethanol was added, and the centrifugation step was repeated twice. Next, the samples were air-dried at room temperature for 5 min, followed by a resuspension in 400 μl of 4% sodium dodecyl sulphate (SDS). Finally, the samples were heat denaturised for 1 h at 60 °C and the protein concentration was measured by the Bradford method using the DC Protein Assay Kit (5000111; Bio-Rad, Hercules, USA). The isolated proteins were separated by SDS-PAGE using 12% polyacrylamide gels and wet-transferred onto nitrocellulose membranes. We used Ponceau-S staining to verify transfer efficiency and determined the total protein as a loading control for protein quantification (Eaton et al., 2013). After rinsing, we pre-blocked the membranes with 5% skim milk and incubated them with primary antibody against anti-Iba1 (1:2000; 019–19741; Wako), occludin (1:500; Ab31721; Abcam), zonula occludens protein-1 (ZO1) (1:500; 5406S; Cell

Signalling) and Tlr4 (1:1000, ab13867, Abcam). For primary antibody detection, we used horseradish peroxidase (HRP) conjugated secondary antibody and the ECL Prime Western Blotting Detection Reagent (RPN2232; GE Healthcare, Chicago, USA). The blots were visualized and documented using a gel imaging system (Amersham Imager 600; GE Healthcare). Protein abundance was densitometrically analysed in ImageJ and normalized using total protein staining (Aldridge et al., 2008; Eaton et al., 2013). For Iba1, occludin and ZO-1, relative protein expression changes were quantified as the difference between WT and TnC$^{-/-}$ animals for each time point separately. To analyse the expression of Tlr4 versus time after stroke, relative protein expression was quantified in WT and TnC$^{-/-}$ animals at 1, 3 and 7 DPI as ratio to naïve WT.

2.10. RT-qPCR

Total RNA was extracted using the RNeasy Mini Kit (74104; Qiagen, Hilden, Germany). The concentration of mRNA was measured using a spectrophotometer (NanoDrop Lite; Thermo Fisher Scientific), and cDNA synthesis was performed using a commercially available kit and random hexamer primers (RevertAid First Strand cDNA Synthesis Kit, K1622; Thermo Fisher Scientific). To analyse Tlr4 expression, 2 ng of cDNA was amplified by RT-qPCR in a Light Cycler 96 (Roche Applied Science, Mannheim, Germany) using the SYBR Select Master Mix and primer pairs for cyclophilin (NM_026352.4; forward: aaggatggcaaggattgaaa; reverse: ctttaagcaattctgcctgga) and Tlr4 (NM_021297.3; forward: ggactctgatcatggcactg; reverse: ctgatccatgcattggtaggt). CT values were normalized using cyclophilin as housekeeping gene. Primer efficiency was tested beforehand, and the relative expression was analysed using the ΔCt method.

2.11. Flow cytometry

Immune cells infiltrating the ischemic brain were analysed by flow cytometry. Ischemic brain hemispheres were manually dissected and immersed in cell maintenance medium (DMEM with 0.01 M HEPES). The tissues were minced using a 70 μm pore cell strainer (352350; Corning Inc, New York, USA) and centrifuged at 400 g for 10 min at room temperature. The supernatant was aspirated and the remaining pellet was resuspended in 37% Percoll (17–0891-02; Merck, Darmstadt, Germany) in 0.01 M HCl/ PBS, followed by centrifugation at $2800g$ for 20 min at room temperature. The supernatant and myelin fraction were carefully aspirated, and the remaining Percoll was washed away. To remove Percoll residues, the samples were again centrifuged at $400g$ for 10 min. Finally, the cell fraction was resuspended in FCM buffer (2% fetal cow serum in PBS, pH 7.4) to prevent the unspecific binding of the antibodies. We verified the viability of recovered cells by trypan blue staining using EVE Automatic Cell Counter (NanoEntek, Waltham, USA) and EVE Cell counting slides (NanoEntek). After removing the excess buffer, cell suspensions were incubated with fluorophore conjugated primary antibodies diluted in FCS buffer for 30 min in the dark at 4 °C. To discriminate the immune cell populations, we used the specific antibodies against CD45, CD3, CD19, CD8, CD11b, Ly6G and Ly6C (see Supplementary Table 2 for details). The number of labelled single cells was quantified with a flow cytometer (Aria III; BD Biosciences, San Jose, USA). Fluorescence minus one (FMO) controls and the gating strategy are shown in Supplementary Fig. 2. Data were analyzed using FlowJo 10.6.0 software (BD Biosciences).

2.12. Statistics

Data were analyzed using Prism 8.0 software (GraphPad, San Diego, USA). Animal mortality was evaluated using the Mantel-Cox Long-rank test. Body weight and neurological score were examined using mixed effects repeated measurement analysis of variance (ANOVA) tests. These data were presented as mean ± S.D. values. Ischemic injury,

immunohistochemistry, Western blots and flow cytometry were analyzed using two-way ANOVA, followed by least significant difference (LSD) tests as posthoc tests. These data were presented as box plots with median (line) and mean (dot) ± interquartile range with minimum/ maximum data points as whiskers. Significance levels were indicated with asterisks.

3. Results

3.1. TnC deficiency does not influence animal survival, neurological deficits and ischemic brain injury

A small number of animals had to be sacrificed given predefined exclusion criteria during the first week post-MCAO, but the survival rate did not differ between WT and $TnC^{-/-}$ mice ($X^2(1, 229) = 1.5$, $p = 0.22$) (Fig. 1A). Using the Clark score, reproducible neurological deficits were noted in ischemic WT and $TnC^{-/-}$ mice at 1 DPI, which decreased over 3 to 7 DPI (Fig. 1B). Neurological deficits during the acute stroke phase correlated with the post-acute brain atrophy (Supplementary Fig. 3) and did not differ between genotypes. Brain infarcts evaluated by cresyl violet (that is, Nissl) staining covered the ischemic striatum and, in approximately one fifth of animals, overlying cortex. Infarct volume did not differ between WT and $TnC^{-/-}$ mice at 1, 3 and 7 DPI (Fig. 1C and Supplementary Fig. 4), nor did brain atrophy or striatum atrophy at 42 DPI (Fig. 1D). Cell death and neuronal death in the ischemic striatum, which is the core of the middle cerebral artery territory, did not differ between both genotypes (Fig. 1E, F), as assessed by TUNEL.

3.2. TnC is de novo expressed in ischemic striatum and, to lesser extent, the perilesional cortex after intraluminal MCAO

Post-MCAO, we observed a strong increase of TnC immunoreactivity in the ischemic striatum and, to lesser extent, the overlying most lateral cerebral cortex at 1 DPI, which remained elevated at similarly high level until 7 DPI (Fig. 2A, B). The area of strongest TnC immunoreactivity coincided with the ischemic lesion and overlapped with regions exhibiting upregulated Iba1 expression. The *de novo* expression of TnC was associated, at least partially, with reactive astrocytes (Supplementary Fig. 5).

3.3. TnC deficiency increases overall Iba1 immunoreactivity in the ischemic brain parenchyma

Immunoreactivity for Iba1 protein is commonly used for detecting the abundance and activity of microglia/macrophages (Ito et al., 2001). Interestingly, Iba1 protein expression was significantly higher in the ischemic hemisphere of $TnC^{-/-}$ compared with WT mice at 7 DPI, as shown by Western blot (Supplementary Fig. 6A, B). The analysis of brain sections revealed that Iba1 immunoreactivity was specifically increased in the perilesional cortex of $TnC^{-/-}$ mice (Fig. 2C-E). This observation indicated that TnC deficiency facilitates the spread of microglia in per-ilesional areas, whereas in WT TnC expression restricts microglial distribution to the lesion core. Of note, the antibody that we used for Iba1 immunohistochemistry detects both resident and activated microglia (Sardari et al., 2020).

3.4. TnC deficiency reduces the cell territories of activated microglia

In the healthy brain, microglia cells occupy non-overlapping territories and actively survey the space allotted to them (Askew et al., 2017; Nimmerjahn et al., 2005). Various inflammatory stimuli, including neuroinflammatory responses post-stroke, induce morphological changes in activated microglia that increase migratory capacity but reduce cell territory (Fernández-Arjona et al., 2017; Lively and Schlichter, 2013). We analysed the 3D morphology of Iba1$^+$ microglia/macrophages in ischemic brain tissue to define whether TnC deficiency
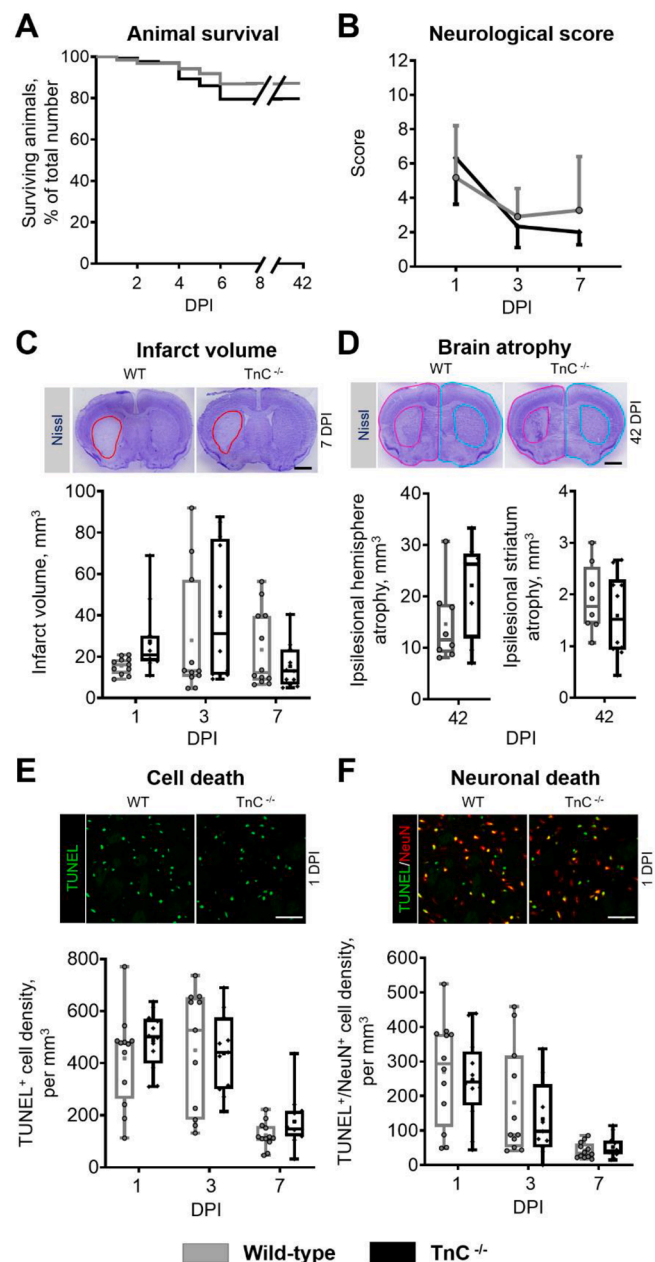

Fig. 1. TnC deficiency does not influence neurological deficits and ischemic injury after intraluminal middle cerebral artery occlusion (MCAO). (A) Animal survival, (B) Clark's neurological score, (C) infarct volume evaluated by cresyl violet (that is, Nissl) staining, (D) brain atrophy and striatum atrophy, (E) cell death in the ischemic striatum evaluated by TUNEL (in green), (F) neuronal death in the ischemic striatum evaluated by NeuN immunolabelling (in red) combined with TUNEL (in green) was evaluated violet in wild type (WT) and $TnC^{-/-}$ mice at different time-points after MCAO. Graphs show percent values (in A), means ± SDs (in B) or box plots with data as dots, means as squares, medians as lines, interquartile ranges as boxes and minimum/ maximum values as whiskers (in C to F). Representative cresyl violet staining of 7 DPI and 42 DPI brains are shown in C, D. Red outline: infarcted area; magenta: ipsilateral hemisphere and striatum; blue: contralateral hemisphere and striatum. No significant differences between genotypes were detected. Scale bar, 1 mm (in C, D) and 50 μm (in E, F). We analysed 119 male wild type (WT) and 110 $TnC^{-/-}$ mice in A and B. In C to F, n = 11 animals per group were enrolled. (For interpretation of the references to colour in this figure legend, the reader is referred to the web version of this article.)
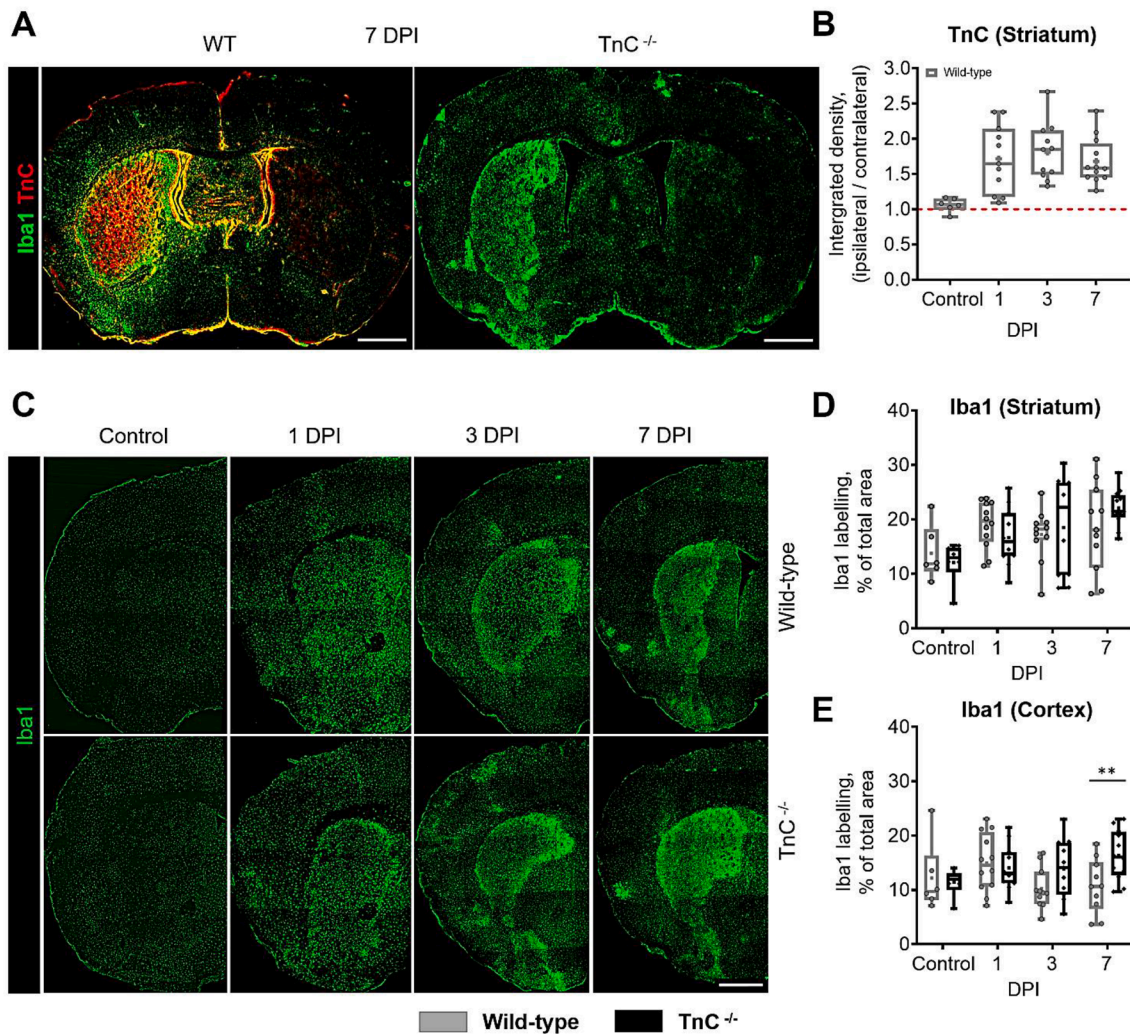
Fig. 2. TnC deficiency increases post-ischemic Iba1 immunoreactivity. (A) Representative immunostaining of Iba1 (in green) and TnC (in red) in the ischemic brain of a WT and TnC$^{-/-}$ mouse exposed to transient intraluminal MCAO at 7 DPI. (B) Quantitative analysis of post stroke TnC immunolabelling in WT animals. (C) Representative Iba1 immunolabelling and (D, E) quantitative analysis of the Iba1 labeled area in the ischemic striatum and cortex for both genotypes at different time-points after transient intraluminal MCAO. Asterisks denote significant differences between genotypes as indicated by two-way ANOVA and Fisher's LSD tests (**p < 0.01), n = 11. Graphs are box plots with data as dots, means as squares, medians as lines, interquartile ranges as boxes and minimum/ maximum values as whiskers. Scale bar, 1 mm. (For interpretation of the references to colour in this figure legend, the reader is referred to the web version of this article.)

affects shape transitions associated with microglial activation. We implemented the recently developed 3DMorph workflow combining high-resolution confocal microscopy and cell shape segmentation (York et al., 2018). To our knowledge, this is the first approach that allows discriminating single cells in densely packed lesions and provides un-biased morphology quantification. For each cell, we analysed the three most relevant parameters of microglia morphology: cell territory, number of branches and cell volume. Cell territory indicates the volume of brain tissue that can be surveyed by a single microglia cell. The number of branches correlates with the exploratory activity of the cell. Cell volume accounts for possible swelling or retraction of perikaryon or processes. In case of microglia, the two characteristic shapes can be detected manually: ramified resting microglia (large cell territory, many branches) and amoeboid cells (small cell territory, few branches, and smaller cell volume). However, a continuum of shape changes lies be-tween these opposing morphologies, requiring a precise and unbiased quantification, which we performed with automated threshold setting and segmentation (Fig. 3A). This procedure allowed us to skeletonize the microglial cells (Fig. 3A) and to study a comprehensive set of morpho-logical metrics in the densely packed ischemic striatum.

The number of microglial cells in the ischemic striatum gradually

increased during the first week post MCAO, but did not differ between genotypes (Fig. 3B). Compared with WT mice, TnC$^{-/-}$ mice exhibited stronger microglial activation at 3 and 7 DPI, indicated by excessive loss of microglial cell territory, branching and volume (Fig. 3C–E). Hence, tissue coverage by microglial cells was reduced in TnC$^{-/-}$ mice (Fig. 3A). These results suggested that the exploratory activity and im-mune surveillance of microglia post-stroke is compromised by TnC deficiency.

3.5. TnC deficiency does not alter post-ischemic expression of Tlr4 protein

TnC represents one of the key endogenous ligands of Tlr4 that reg-ulates microglial migration and phagocytic activity (Haage et al., 2019). We therefore asked how TnC deficiency influenced Tlr4 expression. RT-qPCR measurements showed that *Tlr4* mRNA levels transiently increased in ischemic brains at 1 and 3 DPI, and were elevated in TnC$^{-/-}$ animals at 1 DPI, but did not differ between genotypes at 3 and 7 DPI (Supplementary Fig. 7A). Western blot analysis (Supplementary Fig. 7B, C) revealed no differences in post stroke Tlr4 protein expression be-tween genotypes.
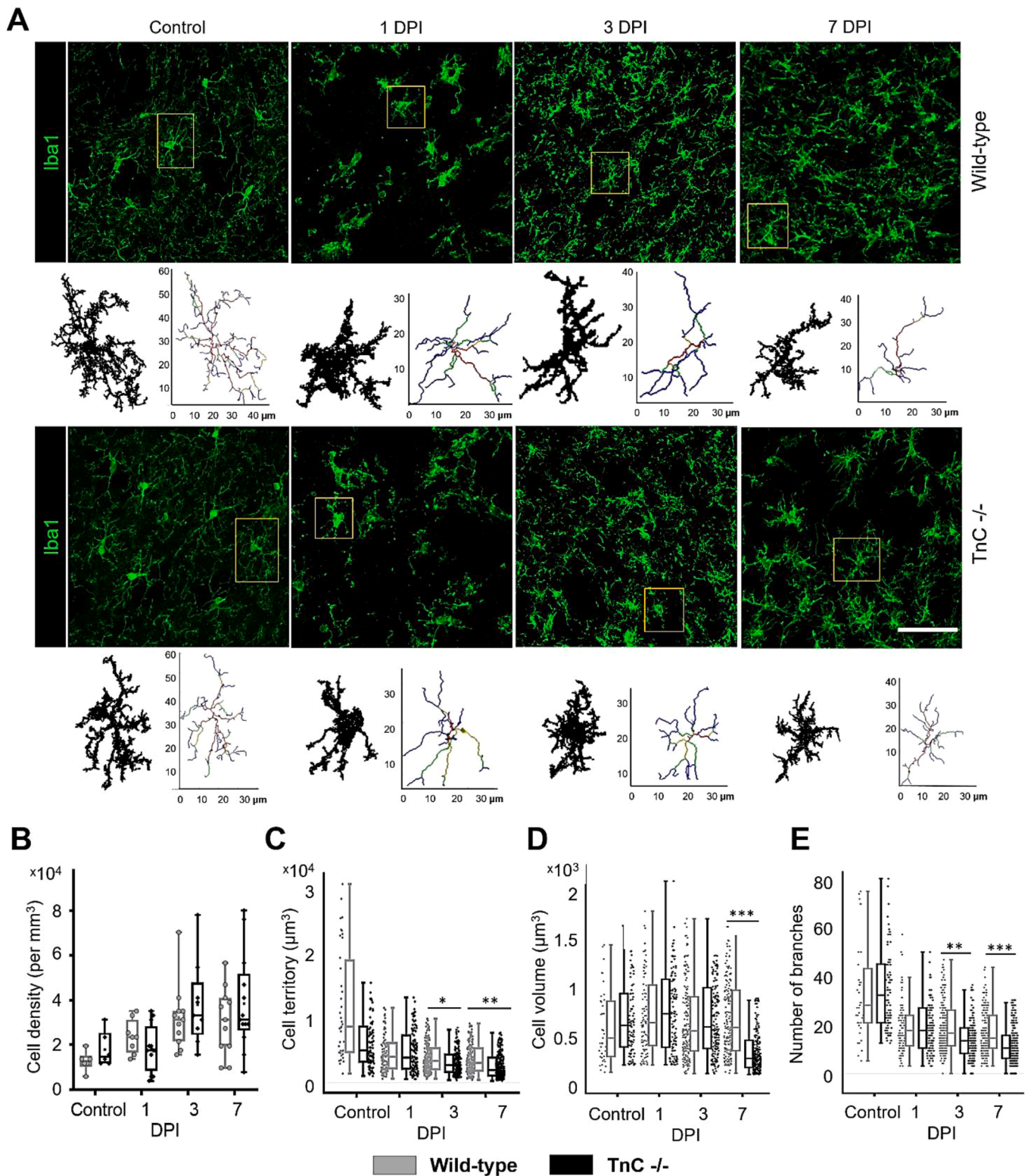
Fig. 3. TnC deficiency compromises post-ischemic tissue surveillance by microglial cells. (A) Morphology analysis of Iba1$^+$ microglia in the ischemic striatum of WT mice and TnC$^{-/-}$ mice at different time-points after transient intraluminal MCAO. The panel shows representative Z-projections of confocal high-resolution 3D stacks, in which single microglial cells were reconstructed, segmented and skeletonized. Examples are highlighted with yellow squares. In the data sets obtained, (B) the density of microglial cells, (C) microglial cell territory, (D) the number of branches per cell and (E) microglial cell volume were calculated at different time-points after transient intraluminal MCAO. Graphs are box plots with data as dots, means as squares, medians as lines, interquartile ranges as boxes and minimum/ maximum values as whiskers. Asterisks denote significant differences between genotypes as indicated by two-way ANOVA and Fisher's LSD tests (*p < 0.05/ **p < 0.01/ ***p < 0.001), n = 11. Scale bar, 50 μm. (For interpretation of the references to colour in this figure legend, the reader is referred to the web version of this article.)

3.6. TnC deficiency does not influence post-ischemic microglia/macrophage proliferation

We next wondered if TnC deficiency influenced the proliferation of microglia in ischemic brain tissue. To evaluate this possibility, we determined the number of proliferating $Ki67^+$ cells and $Ki67^+$/ $Iba1^+$ microglia/macrophages in the ischemic striatum of $TnC^{-/-}$ and WT mice at 3 and 7 DPI. At both time-points, the number of proliferating $Ki67^+$ cells and $Ki67^+$/ $Iba1^+$ cells did not differ between both genotypes (Supplementary Fig. 8).

3.7. TnC deficiency increases leukocyte and, specifically, T cell accumulation in the ischemic brain

Microglial cells vividly interact with leukocytes in the ischemic brain, thereby potentially controlling their access into the ischemic brain parenchyma (Neumann et al., 2015). In view of the reduced microglial surveillance, we examined how TnC deficiency influenced the infiltration of peripheral blood leukocytes into the ischemic brain parenchyma. By CD45 immunohistochemistry we revealed that the number of infiltrated leukocytes was increased in the ischemic striatum of $TnC^{-/-}$ compared with WT mice at 7 DPI (Fig. 4). Infiltrated leukocytes were determined as $CD45^{high}$/$Iba1^{low}$ cells (Supplementary Fig. 9).

In view of these findings, we further analysed the subsets of brain-invading leukocytes by flow cytometry. Cell counts of $CD45^+$ leukocytes were increased in the ischemic brain tissue of $TnC^{-/-}$ compared with WT mice at 3 and 7 DPI (Fig. 5A), supporting the results of immunohistochemical analysis. Among $CD45^+$ leukocytes, $CD3^+$ T cells made up the largest subset (Fig. 5B), of which a smaller percentage was $CD8^+$ (Fig. 5C) and a larger percentage was $CD8^-$ (Fig. 5D). TnC deficiency significantly increased the percentage of T cells and, specifically, $CD8^-$ T cells in the ischemic brain parenchyma (Fig. 5B, D). The percentage of $CD8^+$ T cells (Fig. 5C), $CD19^+$ B cells (Fig. 5E), $CD3^-$/$CD19^-$ myeloid cells (Fig. 5F), $Ly6G^+$/$CD11b^+$ neutrophils (Fig. 5G) and $Ly6C^+$/$CD11b^+$ monocytes (Fig. 5H), on the other hand, did not differ between WT and $TnC^{-/-}$ mice. Our data support a role of TnC in controlling T cell invasion into the ischemic brain.

3.8. TnC deficiency does not affect blood–brain barrier breakdown after stroke

We further hypothesized that the increased infiltration of leukocytes can be driven by the aggravated breakdown of blood–brain barrier (BBB) in $TnC^{-/-}$ mice after stroke. We evaluated such possibility by investigating brain swelling, immunoglobulin (IgG) extravasation, and the abundance of tight junction proteins. Both WT and $TnC^{-/-}$ animals exhibited ipsilateral hemisphere swelling and IgG extravasation at 1 and 3 DPI, indicating dysfunctional BBB (Supplementary Fig. 10A, B). However, we observed no significant differences between genotypes. The abundance of the tight junction proteins occludin (Supplementary Fig. 10C, D) and ZO1 (Supplementary Fig. 10E, F) at 1, 3 and 7 DPI was reduced in both WT and $TnC^{-/-}$ mice, but no significant differences between genotypes were detected. These data suggest that the distinct pattern of microglia/macrophage activation and T-cell infiltration in TnC deficient mice was not associated with major neurovascular abnormalities.

3.9. TnC deficiency does not affect ICAM1/ CD31 association on endothelial cells, but increases ICAM1/ Iba1 co-localization on microglial cells

Post-ischemia, the *de novo* expression of ICAM1 on endothelial cells mediates the infiltration of peripheral blood immune cells into the brain parenchyma (Iadecola and Anrather, 2011). Since we observed the increased number of leukocytes in the ischemic brain of $TnC^{-/-}$ compared with WT mice, we subsequently explored whether TnC deficiency altered the ICAM1's co-localization with CD31 on endothelial cells and Iba1 in microglia/macrophages, respectively. Using Mander's spatial co-localization coefficient M1, we analysed the association of ICAM1 with both markers in the ischemic striatum at 1, 3 and 7 DPI. Notably, the co-localization of ICAM1 and CD31 did not differ between genotypes at all three time-points examined (Supplementary Fig. 11A, B), whereas ICAM1 and Iba1 co-localization increased in the ischemic striatum of $TnC^{-/-}$ compared with WT mice at 7 DPI (Supplementary Fig. 11C, D). We suggest that the increased association of ICAM1 with Iba1 in ischemic brains of TnC deficient mice might represent a surrogate of the increased microglial activation state, making the brain prone for neuroinflammatory responses.

4. Discussion

Using the $TnC^{-/-}$ mice, which we exposed to transient intraluminal MCAO, this study provides the first evidence that TnC controls microglial activation in the ischemic brain, restricting the access of blood-derived leukocytes and, more specifically, T cells into the injured brain parenchyma. Compared with WT mice, $TnC^{-/-}$ mice exhibited a distinct pattern of microglia activation at 3 and 7 DPI, characterized by increased immunoreactivity for Iba1, increased spread of $Iba1^+$
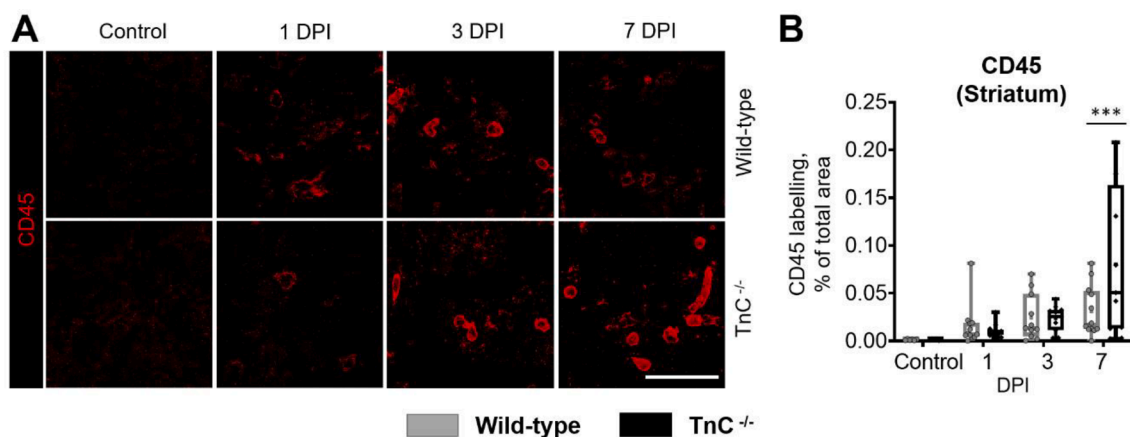

Fig. 4. TnC deficiency increases leukocyte infiltration of the ischemic brain parenchyma. (A) Representative immunohistochemistry and (B) quantitative analysis of $CD45^{high}$/$Iba1^{low}$ leukocytes in the ischemic striatum of WT mice and $TnC^{-/-}$ mice at different time-points after transient intraluminal MCAO. Graphs are box plots with data as dots, means as squares, medians as lines, interquartile ranges as boxes and minimum/ maximum values as whiskers. Asterisks denote significant differences between genotypes as indicated by two-way ANOVA and Fisher's LSD tests (***p < 0.001), n = 11. Scale bar, 50 μm.
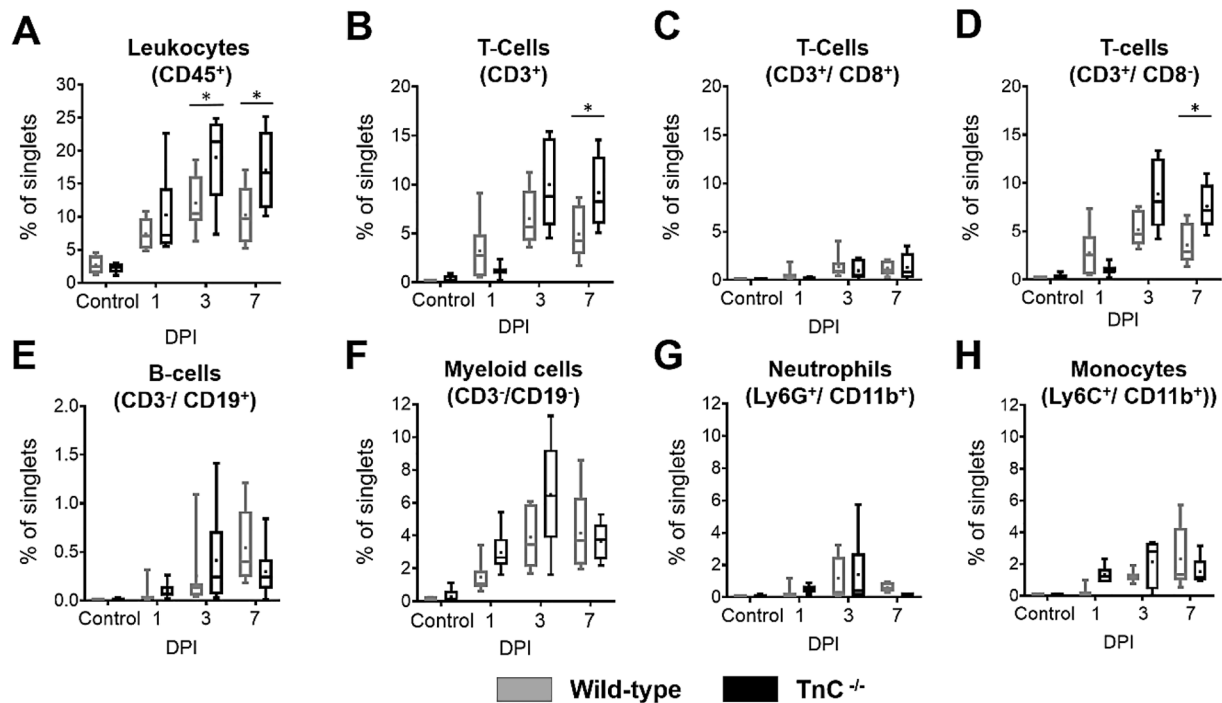
Fig. 5. TnC deficiency elevates leukocyte and, more specifically, T cell counts in the ischemic brain parenchyma. Flow cytometry analysis of (A) total $CD45^+$ leukocyte, (B) $CD3^+$ T cell, (C) $CD8^+/ CD3^+$ T cell, (D) $CD8^-/ CD3^+$ T cell, (E) $CD19^+$ B cell, (F) $CD3^-/ CD19^-$ myeloid cell, (G) $Ly6G^+/ CD11b^+$ neutrophil and (H) $Ly6C^+/ CD11b^+$ monocyte counts of WT mice and $TnC^{-/-}$ mice at different time-points after transient intraluminal MCAO. Asterisks denote significant differences between genotypes as indicated by two-way ANOVA and Fisher's LSD tests (*p < 0.05), n $= 6$.

microglia/macrophages into perilesional brain areas, reduced microglial cell territory, reduced microglial branching and reduced microglial cell volume, as compared with WT mice. As such, the brain tissue surveillance by microglial cells was reduced in $TnC^{-/-}$ compared with WT mice. By flow cytometry we showed an increased number of peripheral blood leukocytes and, specifically $CD8^-/ CD3^+$ T cells in the ischemic brain parenchyma of $TnC^{-/-}$ mice. However, $TnC^{-/-}$ did not affect post-ischemic animal survival, neurological deficits, ischemic injury at 1 to 7 DPI and brain atrophy at 42 DPI.

After brain injury, the upregulation of TnC was reported in subarachnoid haemorrhage (Suzuki et al., 2020), cerebral stab wound (Laywell et al., 1992) and, very recently, retinal ischemia (Reinhard et al., 2017). Here, we observed the concurrent upregulation of TnC and Iba1 in the ischemic striatum of WT mice, suggesting the possible involvement of TnC in controlling sterile neuroinflammation post-MCAO. In neuroinflammation, TnC acts as endogenous activator of Tlr4, inducing microglial chemotaxis, phagocytosis and proinflammatory cytokine production (Haage et al., 2019). However, a number of other ECM molecules bind to Tlr4, including biglycan, hyaluronan, heparan sulphate, high mobility group protein-B1 (HMGB1), fibrinogen and fibronectin (Yu et al., 2010). The expression of Tlr4 was significantly higher in the ischemic brain of $TnC^{-/-}$ compared with WT mice at 1 DPI, but it did not differ between genotypes at 3 and 7 DPI. Therefore, a multitude of other ligands could compensate or even enhance microglial Tlr4 signalling in ischemic stroke under conditions of TnC deficiency.

Microglial morphology analyses in 3D revealed that $TnC^{-/-}$ enhanced the loss of microglial cell territory and microglial branching at 3 and 7 DPI, whereas microglial cell number and microglial proliferation were unaltered by $TnC^{-/-}$. This result indicates diminished tissue surveillance by microglial cells in TnC deficient mice exposed to stroke. In light of these studies, the activated microglia is likely to play a role in restricting peripheral blood leukocyte and, more specifically, T cell invasion post stroke. This mechanism requires the direct interaction between microglia and leukocytes that involves adhesion molecules such

as ICAM1. Interestingly, ICAM1 revealed increased co-localization with Iba1 on microglia in $TnC^{-/-}$ compared with WT mice, indicative of a pro-inflammatory microglial state evoked by TnC deficiency. The microglial responses induced by TnC deficiency and their consequences for brain leukocyte recruitment are summarized in Fig. 6.

By immunohistochemistry and flow cytometry we show that $CD45^+$ leukocytes and, more specifically, $CD8^-/ CD3^+$ T cells exhibited increased accumulation in the ischemic brain tissue of $TnC^{-/-}$ compared with WT mice. Interestingly, a similar effect was observed after spinal cord injury (Schreiber et al., 2013). We suggest that the reduced tissue coverage by microglial cells results in the decreased capability to restrict or phagocyte infiltrated leukocytes. The contribution of T cells is well established in ischemic stroke models (Liesz et al., 2011; Mracsko et al., 2014; Neumann et al., 2015). Besides $CD8^+$ T cells, interleukin-17-producing γδ T cells were shown to contribute to ischemic brain injury (Arunachalam et al., 2017), while $FoxP3^+$ regulatory T cells were shown to protect against ischemic damage (Liesz et al., 2009) and promote neurological recovery (Ito et al., 2019). Recently, *in vivo* imaging experiments demonstrated the capability of microglia to engulf and phagocyte infiltrated neutrophils in ischemic brain parenchyma (Neumann et al., 2018; Otxoa-de-Amezaga et al., 2019). It is not unlikely that a similar process contributed to the clearance of T cells from the ischemic brain.

In this study, implementing the new method of cell morphology analysis allowed for the measurement of single microglia cells within the densely packed ischemic brain lesion. This was possible because in comparison with previously established methods (Heindl et al., 2018), our approach does not require nuclear staining, which often fails to identify single cells inside the infarct core. Here we focused on deciphering the impact of TnC on microglia morphology after stroke, but the roles of other extracellular molecules and structural alterations in other cell types can similarly be evaluated by morphology analysis. The association between TnC and reactive astrocytes indicates the necessity to further investigate the consequences of ECM changes for astrocytic morphology in the ischemic brain. It will be also important to
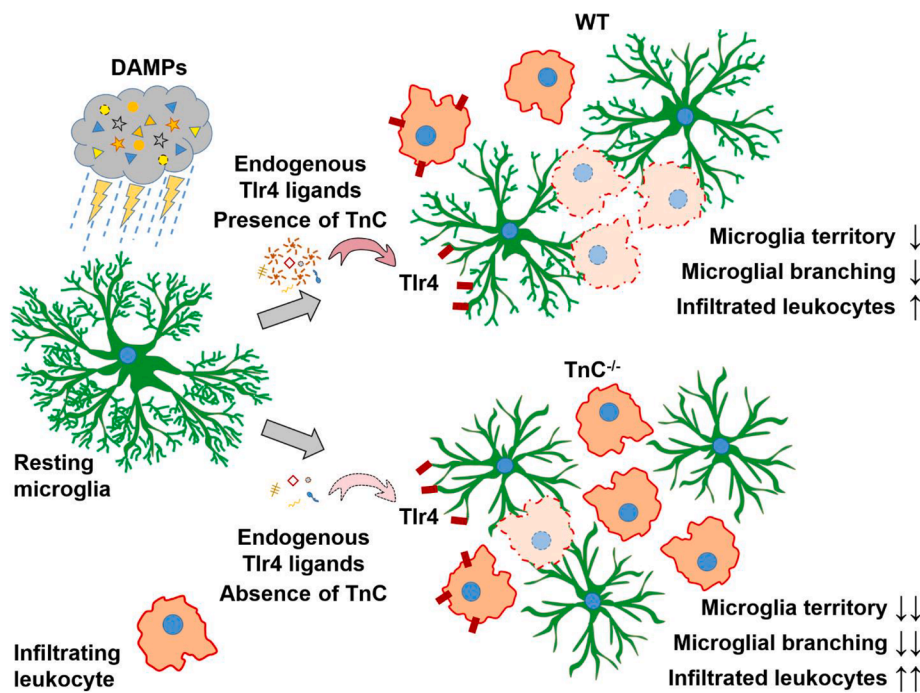
Fig. 6. Role of TnC in post-ischemic microglial activation and neuroinflammation. In ischemic stroke, the release of damage-associated patterns (DAMPs) activates microglial cells, assisted by endogenous toll-like receptor-4 (Tlr4) ligands. In WT mice, the tissue coverage by activated microglia is sufficient to survey the injured tissue. This restricts the entry of peripheral leukocytes (comprising T cells) into the ischemic brain. In TnC deficient mice, the reduced microglial surveillance augments the leukocyte (specifically T cell) accumulation in the ischemic brain.

understand how ECM affects stroke recovery in the context of microglia depletion (Szalay et al., 2016) or anti-inflammatory treatments. To improve the translational value of future studies, intraluminal MCAO and thromboembolic stroke (Chen et al., 2015; Kilic et al., 1998) models can be used.

5. Conclusion

Although the deficiency of TnC did not affect cell death and neurological deficits during the first week after focal cerebral ischemia, TnC deficiency potently influenced post-ischemic immune responses. The loss of microglial surveillance territory in TnC deficient mice went along with the increased accumulation of infiltrated peripheral blood leukocytes and, specifically, T cells in the ischemic brain. The observed changes in microglia activation raise the necessity of studying the effects of endogenous Tlr4 ligands and ECM components on post-ischemic brain remodelling and stroke recovery.

Acknowledgement

Appendix A. Supplementary data

Supplementary data to this article can be found online at https://doi.org/10.1016/j.bbi.2020.10.016.

References

Aldridge, G.M., Podrebarac, D.M., Greenough, W.T., Weiler, I.J., 2008. The use of total protein stains as loading controls: an alternative to high-abundance single-protein controls in semi-quantitative immunoblotting. J. Neurosci. Methods 172, 250–254.

Anrather, J., Iadecola, C., 2016. Inflammation and stroke: an overview. Neurotherapeutics 13, 661–670.

Arunachalam, P., Ludewig, P., Melich, P., Arumugam, T.V., Gerloff, C., Prinz, I., Magnus, T., Gelderblom, M., 2017. CCR6 (CC chemokine receptor 6) is essential for the migration of detrimental natural interleukin-17-producing γδ T cells in stroke. Stroke 48, 1957–1965.

Askew, K., Li, K., Olmos-Alonso, A., Garcia-Moreno, F., Liang, Y., Richardson, P., Tipton, T., Chapman, M.A., Riecken, K., Beccari, S., Sierra, A., Molnár, Z., Cragg, M.S., Garaschuk, O., Perry, V.H., Gomez-Nicola, D., 2017. Coupled proliferation and apoptosis maintain the rapid turnover of microglia in the adult brain. Cell Rep. 18, 391–405.

Bianchi, M.E., 2007. DAMPs, PAMPs and alarmins: all we need to know about danger. J. Leukoc. Biol. 81, 1–5.

Caso, J.R., Pradillo, J.M., Hurtado, O., Lorenzo, P., Moro, M.A., Lizasoain, I., 2007. Toll-like receptor 4 is involved in brain damage and inflammation after experimental stroke. Circulation 115, 1599–1608.

Chen, Y., Zhu, W., Zhang, W., Libal, N., Murphy, S.J., Offner, H., Alkayed, N.J., 2015. A novel mouse model of thromboembolic stroke. J. Neurosci. Methods 256, 203–211.

Clark, W., Lessov, N., Dixon, M., Eckenstein, F., 1997. Monofilament intraluminal middle cerebral artery occlusion in the mouse. Neurol. Res. 19, 641–648.

Dzyubenko, E., Manrique-Castano, D., Kleinschnitz, C., Faissner, A., Hermann, D.M., 2018a. Role of immune responses for extracellular matrix remodeling in the ischemic brain. Ther. Adv. Neurol. Disord. 11, 1756286418818092.

Dzyubenko, E., Manrique-Castano, D., Kleinschnitz, C., Faissner, A., Hermann, D.M., 2018b. Topological remodeling of cortical perineuronal nets in focal cerebral ischemia and mild hypoperfusion. Matrix Biol. 74, 121–132.

Eaton, S.L., Roche, S.L., Llavero Hurtado, M., Oldknow, K.J., Farquharson, C., Gillingwater, T.H., Wishart, T.M., 2013. Total protein analysis as a reliable loading control for quantitative fluorescent western blotting. PLoS ONE 8, e72457.

Faissner, A., Kruse, J., 1990. J1/tenascin is a repulsive substrate for central nervous system neurons. Neuron 5, 627–637.

Faissner, A., Roll, L., Theocharidis, U., 2017. Tenascin-C in the matrisome of neural stem and progenitor cells. Mol. Cell. Neurosci. 81, 22–31.

Fernández-Arjona, M.D.M., Grondona, J.M., Granados-Durán, P., Fernández-Llebrez, P., López-Ávalos, M.D., 2017. Microglia morphological categorization in a rat model of neuroinflammation by hierarchical cluster and principal components analysis. Front. Cell. Neurosci. 11, 235.

Forsberg, E., Hirsch, E., Fröhlich, L., Meyer, M., Ekblom, P., Aszodi, A., Werner, S., Fässler, R., 1996. Skin wounds and severed nerves heal normally in mice lacking tenascin-C. Proc. Natl. Acad. Sci. 93, 6594–6599.

Gelderblom, M., Leypoldt, F., Steinbach, K., Behrens, D., Choe, C.U., Siler, D.A., Arumugam, T.V., Orthey, E., Gerloff, C., Tolosa, E., Magnus, T., 2009. Temporal and spatial dynamics of cerebral immune cell accumulation in stroke. Stroke 40, 1849–1857.

Haage, V., Elmadany, N., Roll, L., Faissner, A., Gutmann, D.H., Semtner, M., Kettenmann, H., 2019. Tenascin C regulates multiple microglial functions involving TLR4 signaling and HDAC1. Brain Behav. Immun. 81, 470–483.

Heindl, S., Gesierich, B., Benakis, C., Llovera, G., Duering, M., Liesz, A., 2018. Automated morphological analysis of microglia after stroke. Front. Cell. Neurosci. 12.

Iadecola, C., Anrather, J., 2011. The immunology of stroke: from mechanisms to translation. Nat. Med. 17, 796.

Ito, M., Komai, K., Mise-Omata, S., Iizuka-Koga, M., Noguchi, Y., Kondo, T., Sakai, R., Matsuo, K., Nakayama, T., Yoshie, O., Nakatsukasa, H., Chikuma, S., Shichita, T., Yoshimura, A., 2019. Brain regulatory T cells suppress astrogliosis and potentiate neurological recovery. Nature 565, 246–250.

Ito, D., Tanaka, K., Suzuki, S., Dembo, T., Fukuuchi, Y., 2001. Enhanced expression of Iba1, ionized calcium-binding adapter molecule 1, after transient focal cerebral ischemia in rat brain. Stroke 32, 1208–1215.

Jayaraj, R.L., Azimullah, S., Beiram, R., Jalal, F.Y., Rosenberg, G.A., 2019. Neuroinflammation: friend and foe for ischemic stroke. J. Neuroinflamm. 16, 142.

Kazanis, I., Belhadi, A., Faissner, A., C. ffrench-Constant., 2007. The adult mouse subependymal zone regenerates efficiently in the absence of Tenascin-C. J. Neurosci. 27, 13991–13996.

Kilic, E., Hermann, D.M., Hossmann, K.-A., 1998. A reproducible model of thromboembolic stroke in mice. NeuroReport 9, 2967–2970.

Laywell, E.D., Dörries, U., Bartsch, U., Faissner, A., Schachner, M., Steindler, D.A., 1992. Enhanced expression of the developmentally regulated extracellular matrix molecule tenascin following adult brain injury. Proc. Natl. Acad. Sci. 89, 2634–2638.

Liesz, A., Suri-Payer, E., Veltkamp, C., Doerr, H., Sommer, C., Rivest, S., Giese, T., Veltkamp, R., 2009. Regulatory T cells are key cerebroprotective immunomodulators in acute experimental stroke. Nat. Med. 15, 192–199.

Liesz, A., Zhou, W., Mracskó, É., Karcher, S., Bauer, H., Schwarting, S., Sun, L., Bruder, D., Stegemann, S., Cerwenka, A., Sommer, C., Dalpke, A.H., Veltkamp, R., 2011. Inhibition of lymphocyte trafficking shields the brain against deleterious neuroinflammation after stroke. Brain 134, 704–720.

Lively, S., Schlichter, L.C., 2013. The microglial activation state regulates migration and roles of matrix-dissolving enzymes for invasion. J. Neuroinflamm. 10, 75.

Lopes Pinheiro, M.A., Kooij, G., Mizee, M.R., Kamermans, A., Enzmann, G., Lyck, R., Schwaninger, M., Engelhardt, B., de Vries, H.E., 2016. Immune cell trafficking across the barriers of the central nervous system in multiple sclerosis and stroke. Biochim. Biophys. Acta (BBA) – Mol. Basis Dis. 1862, 461–471.

Midwood, K., Sacre, S., Piccinini, A.M., Inglis, J., Trebaul, A., Chan, E., Drexler, S., Sofat, N., Kashiwagi, M., Orend, G., Brennan, F., Foxwell, B., 2009. Tenascin-C is an endogenous activator of Toll-like receptor 4 that is essential for maintaining inflammation in arthritic joint disease. Nat. Med. 15, 774–780.

Mracsko, E., Liesz, A., Stojanovic, A., Lou, W.P., Osswald, M., Zhou, W., Karcher, S., Winkler, F., Martin-Villalba, A., Cerwenka, A., Veltkamp, R., 2014. Antigen dependently activated cluster of differentiation 8-positive T cells cause perforin-mediated neurotoxicity in experimental stroke. J. Neurosci. 34, 16784–16795.

Neumann, J., Riek-Burchardt, M., Herz, J., Doeppner, T.R., König, R., Hütten, H., Etemire, E., Männ, L., Klingberg, A., Fischer, T., Görtler, M.W., Heinze, H.J., Reichardt, P., Schraven, B., Hermann, D.M., Reymann, K.G., Gunzer, M., 2015. Very-late-antigen-4 (VLA-4)-mediated brain invasion by neutrophils leads to interactions with microglia, increased ischemic injury and impaired behavior in experimental stroke. Acta Neuropathol. 129, 259–277.

Neumann, J., Henneberg, S., von Kenne, S., Nolte, N., Müller, A.J., Schraven, B., Görtler, M.W., Reymann, K.G., Gunzer, M., Riek-Burchardt, M., 2018. Beware the intruder: real time observation of infiltrated neutrophils and neutrophil—Microglia interaction during stroke in vivo. PLoS ONE 13, e0193970.

Nimmerjahn, A., Kirchhoff, F., Helmchen, F., 2005. Resting microglial cells are highly dynamic surveillants of brain parenchyma in vivo. Science 308, 1314–1318.

Otxoa-de-Amezaga, A., Miró-Mur, F., Pedragosa, J., Gallizioli, M., Justicia, C., Gaja-Capdevila, N., Ruíz-Jaen, F., Salas-Perdomo, A., Bosch, A., Calvo, M., Márquez-Kisinousky, L., Denes, A., Gunzer, M., Planas, A.M., 2019. Microglial cell loss after ischemic stroke favors brain neutrophil accumulation. Acta Neuropathol. 137, 321–341.

Paul, C.A., Beltz, B., Berger-Sweeney, J., 2008. The nissl stain: a stain for cell bodies in brain sections. Cold Spring Harbor Protoc. pdb.prot4805.

Reinhard, J., Renner, M., Wiemann, S., Shakoor, D.A., Stute, G., Dick, H.B., Faissner, A., Joachim, S.C., 2017. Ischemic injury leads to extracellular matrix alterations in retina and optic nerve. Sci. Rep. 7, 43470.

Roth, S., Singh, V., Tiedt, S., Schindler, L., Huber, G., Geerlof, A., Antoine, D.J., Anfray, A., Orset, C., Gauberti, M., Fournier, A., Holdt, L.M., Harris, H.E., Engelhardt, B., Bianchi, M.E., Vivien, D., Haffner, C., Bernhagen, J., Dichgans, M., Liesz, A., 2018. Brain-released alarmins and stress response synergize in accelerating atherosclerosis progression after stroke. Sci. Transl. Med. 10, eaao1313.

Sardari, M., Dzyubenko, E., Schmermund, B., Yin, D., Qi, Y., Kleinschnitz, C., Hermann, D.M., 2020. Dose-dependent microglial and astrocytic responses associated with post-ischemic neuroprotection after lipopolysaccharide-induced sepsis-like state in mice. Front. Cell. Neurosci. 14, 26.

Schreiber, J., Schachner, M., Schumacher, U., Lorke, D.E., 2013. Extracellular matrix alterations, accelerated leukocyte infiltration and enhanced axonal sprouting after spinal cord hemisection in tenascin-C-deficient mice. Acta Histochem. 115, 865–878.

Shiba, M., Suzuki, H., 2019. Lessons from tenascin-C knockout mice and potential clinical application to subarachnoid hemorrhage. Neural Regener. Res. 14, 262–264.

Stauffer, W., Sheng, H., Lim, H.N., 2018. EzColocalization: An ImageJ plugin for visualizing and measuring colocalization in cells and organisms. Sci. Rep. 8, 15764.

Suzuki, H., Fujimoto, M., Kawakita, F., Liu, L., Nakatsuka, Y., Nakano, F., Nishikawa, H., Okada, T., Kanamaru, H., Imanaka-Yoshida, K., Yoshida, T., Shiba, M., 2020. Tenascin-C in brain injuries and edema after subarachnoid hemorrhage: findings from basic and clinical studies. J. Neurosci. Res. 98, 42–56.

Szalay, G., Martinecz, B., Lénárt, N., Környei, Z., Orsolits, B., Judák, L., Császár, E., Fekete, R., West, B.L., Katona, G., Rózsa, B., Dénes, Á., 2016. Microglia protect against brain injury and their selective elimination dysregulates neuronal network activity after stroke. Nat. Comm. 7, 11499.

Wang, Y.C., Dzyubenko, E., Sanchez-Mendoza, E.H., Sardari, M., Silva de Carvalho, T., Doeppner, T.R., Kaltwasser, B., Machado, P., Kleinschnitz, C., Bassetti, C.L., Hermann, D.M., 2018. Postacute delivery of GABAA alpha5 antagonist promotes postischemic neurological recovery and peri-infarct brain remodeling. Stroke 49, 2495–2503.

Wang, C., Börger, V., Sardari, M., Murke, F., Skuljec, J., Pul, R., Hagemann, N., Dzyubenko, E., Dittrich, R., Gregorius, J., Hasenberg, M., Kleinschnitz, C., Popa-Wagner, A., Doeppner, T.R., Gunzer, M., Giebel, B., Hermann, D.M., 2020. Mesenchymal stromal cell-derived small extracellular vesicles induce ischemic neuroprotection by modulating leukocytes and specifically neutrophils. Stroke 51, 1825–1834.

Wiemann, S., Reinhard, J., Faissner, A., 2019. Immunomodulatory role of the extracellular matrix protein tenascin-C in neuroinflammation. Biochem. Soc. Trans. 47, 1651–1660.

York, E.M., LeDue, J.M., Bernier, L.P., MacVicar, B.A., 2018. 3DMorph automatic analysis of microglial morphology in three dimensions from ex vivo and in vivo imaging. eNeuro 5, 0266–18.2018.

Yu, L., Wang, L., Chen, S., 2010. Endogenous toll-like receptor ligands and their biological significance. J. Cell. Mol. Med. 14, 2592–2603.